



Pathways and watermass transformation of Atlantic Water entering the Nordic Seas through Denmark Strait in two high resolution ocean models

S.L. Ypma^{a,*}, N. Brüggemann^b, S. Georgiou^a, P. Spence^c, H.A. Dijkstra^d, J.D. Pietrzak^a, C.A. Katsman^a

^a Department of Hydraulic Engineering, Delft University of Technology, Civil Engineering and Geosciences, Environmental Fluid Mechanics, Stevinweg 1, 2628 CN Delft, Netherlands

^b Faculty of Mathematics, Informatics and Natural Sciences, University of Hamburg, Hamburg, Germany

^c Climate Change Research Centre, University of New South Wales, Sydney, New South Wales, Australia

^d Institute for Marine and Atmospheric Research Utrecht, Utrecht University, Netherlands



ARTICLE INFO

Keywords:

North Icelandic Irminger Current
North Icelandic Jet
Denmark Strait Overflow Water
Water mass transformation
Nordic Seas
Atlantic Water pathways

ABSTRACT

The pathways and watermass transformation of the North Icelandic Irminger Current (NIIC) in the Nordic Seas are investigated by tracing the NIIC watermass in two ocean circulation models: the Modular Ocean Model (MOM) and the Parallel Ocean Program (POP). The two simulations use identical atmospheric forcing and have a horizontal resolution of 0.1°. However, the models differ strongly in their representation of the sea-ice cover in the Nordic Seas and, possibly as a consequence, display a different hydrography. Results from observational studies point towards a fast overturning loop north of Iceland that connects the NIIC watermass to the Denmark Strait Overflow Water (DSOW). However, our Lagrangian analysis shows that only 0.2 Sv of the entering NIIC water exits as DSOW in the two models. In POP, the main transformation to dense water takes place along a short path north of Iceland. In MOM however, the contributing part of the NIIC to DSOW takes a long path through the Nordic Seas and reaches Denmark Strait as part of the East Greenland Current (EGC). A small contribution of the NIIC watermass to the Iceland Scotland Overflow Water (ISOW) is found in both MOM and POP (7.8%, respectively 2.1% of the NIIC watermass). In the model simulations studied, the part of the NIIC watermass that is not connected to the overflows takes many different pathways through the Nordic seas. Analysis of the depth distribution and the thermohaline changes of the particles indicates that the watermass transformation that takes place north of Iceland is crucial for diversifying the pathways of the NIIC water.

1. Introduction

The transformation of Atlantic Water (AW) north of the Greenland-Scotland Ridge is one of the key mechanisms for controlling the strength of the Atlantic Meridional Overturning Circulation (AMOC) via the overflows through Denmark Strait and across the Iceland-Scotland Ridge. The warm AW flows poleward into the Nordic Seas and beyond through three main gateways (see schematic in Fig. 1) (e.g. Hansen and Østerhus, 2000). Two of these, through which the majority of the AW flows north, are located east of Iceland. West of Iceland, AW is transported by the North Icelandic Irminger Current (NIIC). This third branch flows north along the western Icelandic slope and has been monitored since 1985 (e.g. Jónsson and Valdimarsson, 2005), though the fate of the NIIC has only recently been studied in more detail. Water mass transformation of the AW in the NIIC is thought to be linked to the

densest part of the Denmark Strait Overflow Water (DSOW) (Våge et al., 2011). However, as of yet it is unclear which path the NIIC takes after entering the Nordic Seas and where watermass transformation from the NIIC to DSOW takes place. The aim of this study is to investigate the paths and watermass transformation of the NIIC in detail in two ocean models using a Lagrangian approach.

Previous studies suggest three possible pathways for the NIIC. The first path was described by Swift and Aagaard (1981) as well as Jónsson (1992), who observed Atlantic Water at the north Icelandic continental shelf, without any propagation into the central Iceland Sea. They found that east of Iceland the water leaves the shelf and propagates in the direction of the Norwegian Sea. Stefánsson (1962) showed that part of the NIIC watermass mixes with surface water from the Iceland Sea, forming a watermass that connects to the Iceland Scotland Overflow Water (ISOW).

* Corresponding author.

E-mail address: s.lypma@tudelft.nl (S.L. Ypma).

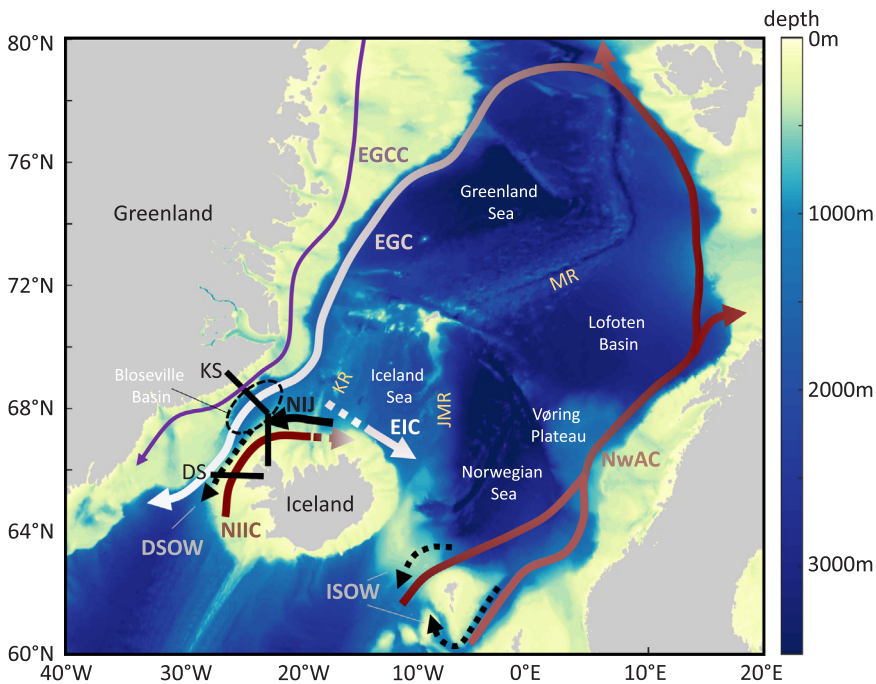


Fig. 1. Schematic of the circulation in the Nordic Seas and bathymetry. Shown in red are the warm and salty inflowing currents: the North Icelandic Irminger Current (NIIC) and the Norwegian Atlantic Current (NwAC). The East Greenland Current (EGC) and the East Icelandic Current (EIC) are shown in white and the East Greenland Coastal Current (EGCC) in purple. Dense currents are shown in black: the North Iceland Jet (NIJ), the Denmark Strait Overflow Waters (DSOW, dashed line) and the Iceland Scotland Overflow Waters (ISOW, dashed lines). The bathymetric features pertinent for this study are indicated in yellow: the Kolbeinsey Ridge (KR), the Jan Mayen Ridge (JMR) and the Mohn Ridge (MR). The release location of the particles at 66° N in Denmark Strait (DS) and the Kögur Section (KS) are shown in black. Note that the bathymetry is from ETOPO2v2, and not the model bathymetry (For interpretation of the references to color in this figure legend, the reader is referred to the web version of this article).

ISOW, which has a similar magnitude as DSOW, is formed by a mixture of watermasses that, combined, are generally labelled as Modified East Icelandic Water (MEIW). The main constituents of the MEIW are the North Icelandic Winter Water, the East Icelandic Water, the Norwegian Sea Deep Water and the Norwegian North Atlantic Water, where the latter is partly formed by transformation of the NIIC watermass (e.g. Hansen and Østerhus, 2000). The main outlet of these watermasses is through the Faroe-Shetland Channel.

Using surface drifters, Valdimarsson and Malmberg (1999) observed a second possible path for the NIIC, where most of their drifters seemed to be topographically steered northward by the Kolbeinsey Ridge (see Fig. 1) and returned south through Denmark Strait in the East Greenland Current (EGC).

More recently, analyses from multiple hydrographic transects along the coast of Iceland suggested a third possible pathway. They point to a close relationship between the NIIC and the North Icelandic Jet (NIJ) (e.g. Våge et al., 2011, 2013, 2015). The NIJ transports the densest component of the Overflow Water through Denmark Strait (Våge et al., 2011). The other two currents advecting dense water from the north through the strait are the shelf break current and the separated branch of the EGC (Harden et al., 2016). The observations show several indications of a connection between the NIIC and the NIJ. First, both currents can be traced along the continental slope of Iceland until their signal disappears at the northeast corner of the island (Våge et al., 2011). Along the Icelandic shelf, the currents seem to be dynamically linked by sharing a pronounced density front (Pickart et al., 2017). Second, the volume transport of both currents is very similar. It is estimated to be 1 Sv and 0.88 Sv for the NIJ and NIIC, respectively (Jónsson and Valdimarsson, 2012; Harden et al., 2016).

Våge et al. (2011) showed, by using an idealized model set-up, that the mechanism that links the NIIC and the NIJ is similar to the one described by e.g. Spall (2004) and Straneo (2006). These studies suggest that buoyant water from the NIIC is transported to the interior of the Iceland Sea by eddies due to baroclinic instability of the NIIC. In these idealized models, the heat flux from the boundary current to the interior balances the atmospheric cooling over the interior that induces convection. The dense watermass returns to the Icelandic slope where it sinks and forms the NIJ.

So far, follow-up studies have not been able to corroborate the connection between the NIIC and the interior of the Iceland Sea. Using

measurements from eight shipboard surveys, Pickart et al. (2017) find a strong, in phase correlation in salinity between the NIJ and NIIC. In case the two currents are linked, this would imply the existence of a very fast overturning. To accommodate this short time-scale, they hypothesize that the overturning can not take place in the central Iceland gyre, but instead takes place northwest of the gyre where deep mixed layers are observed. In their discussion it remains unclear how the water of the NIIC reaches this area. Additionally, de Jong et al. (2018) do not find a connection between the interior Iceland Sea and the NIJ either. In their study, based on the analysis of deployed RAFOS floats, they highlight the importance of the East Icelandic Current (EIC, Fig. 1) that potentially blocks the exchange between the Iceland Sea gyre and the Icelandic slope region. This branch might not be captured by the idealized model of Våge et al. (2011). Tracking the NIJ watermass back in time in a high resolution ocean model (Viking20) leads to a similar insight: no exchange with the interior of the Iceland Sea is seen and most of the NIJ originates from the shelfbreak EGC (Behrens et al., 2017). It is therefore still unclear what role the NIIC plays for the formation of Denmark Strait Overflow Waters.

Lagrangian studies as Behrens et al. (2017) can be very useful as particle tracking in global ocean models has the advantage that a large number of particles can be used in comparison to observations, providing better statistics of variable pathways. However, different ocean models lead to different conclusions. For example, backtracking the overflow waters in the 1/20° horizontal resolution Viking20 ocean model, Behrens et al. (2017) find that the bulk part of the Denmark Strait Overflow Water in the model (60%) has an Arctic origin. In contrast, in the 1/10° ocean model used by Köhl (2010) the largest part of the DSOW originates from watermass transformation taking place within the Nordic Seas. Köhl (2010) argues that the pathways vary spatially depending on the magnitude of the wind stress. Thus, he concluded that the differences in ocean models regarding forcing and set-up may lead to significantly different results.

In addition to the variables mentioned by Köhl (2010), the horizontal resolution, discretization in the vertical, topography, mixing parameterizations and boundary conditions like applied atmospheric forcing and sea-ice conditions impact the mixed layer dynamics and therefore the circulation in the models (Willebrand et al., 2001; Langehaug et al., 2012; Courtois et al., 2017). A correct representation of the convection regions is crucial for the transformation processes of

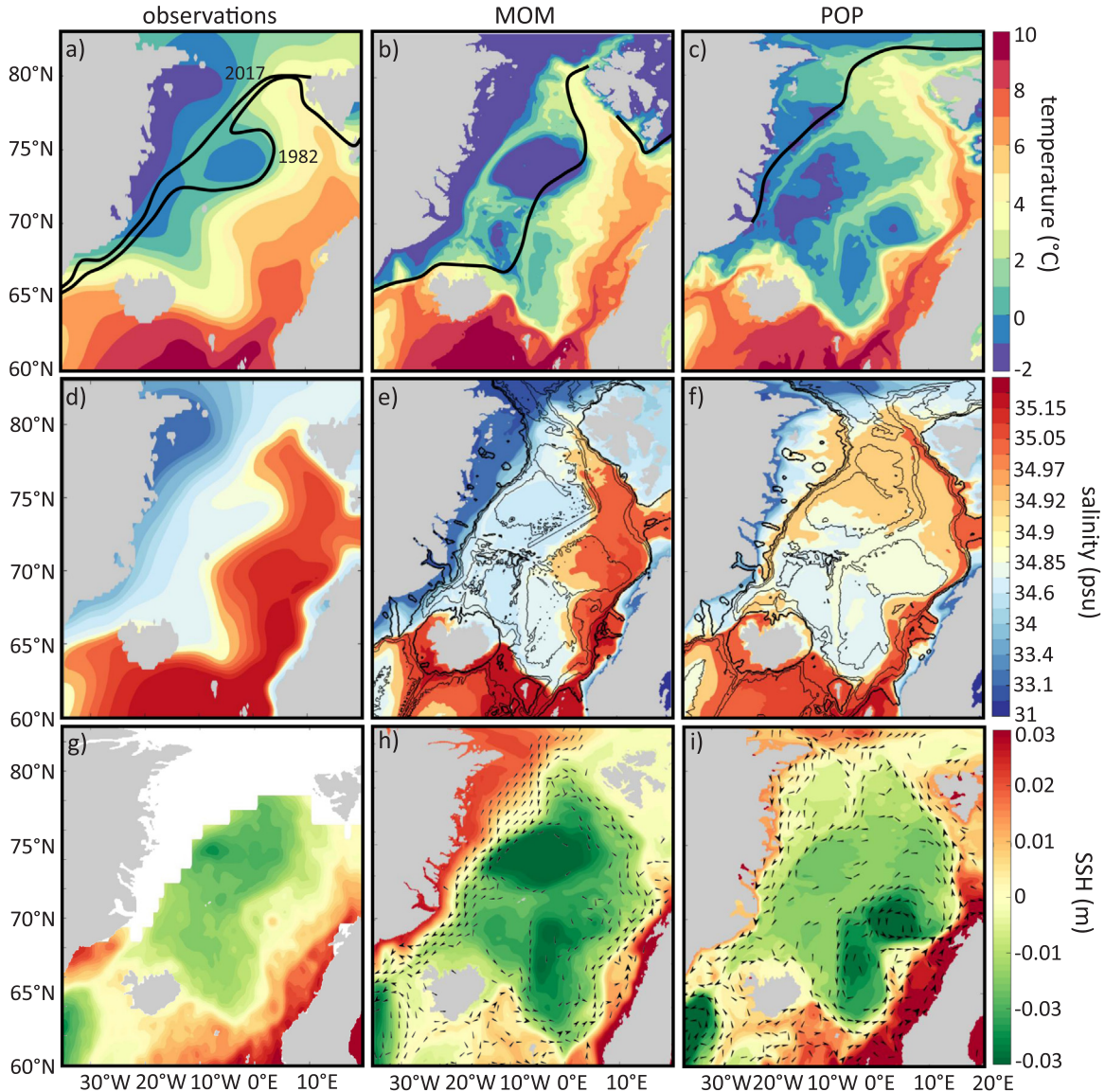


Fig. 2. Mean temperature (top) and salinity (middle) at 50 m depth and sea surface height (bottom) from (a,d,g) observations, (b,e,h) MOM and (c,f,i) POP. The observational hydrographic fields show the mean from 1995 to 2010 and are obtained from the Climatological Atlas of the Nordic Seas (Korablev et al., 2014). Panel (g) shows the mean absolute dynamic topography over the same period from the AVISO satellite altimetry. The black lines in (a-c) indicate the sea-ice extent in March. In (a) the extent in 1982 and 2017 are shown from the Sea Ice Index (Fetterer et al., 2017). The contour lines in (e) and (f) show the model isobaths at 400 m (thick black line), 1000 m, 1500 m and 3000 m depth. The black arrows in (h) and (i) show the mean surface velocity field for flow stronger than 0.05 m/s.

watermasses. However, ocean models still show large differences in mixed layer depth, both in low- and high resolution ocean models (e.g. Tréguier et al., 2005; Danabasoglu et al., 2014).

The aim of this study is to investigate to what extent the inflowing Atlantic Water through Denmark Strait contributes to the Overflow Water and whether its transformation is related to the location of convection regions within the Nordic Seas as proposed by Våge et al. (2011). A Lagrangian perspective is chosen, where the NIIC watermass entering the Nordic Seas through Denmark Strait is tracked in two ocean models that differ substantially in their representation of deep convection: the Modular Ocean Model (MOM) and the Parallel Ocean Program (POP). The models have the same horizontal grid with a resolution of 0.1° and identical atmospheric forcing. However, their sea-ice representation and consequently the hydrography in the Nordic Seas is different. This paper presents the pathways of the NIIC water in these two models, a quantification of the contribution of the NIIC to the overflows and a discussion on where and how the NIIC watermass is transformed.

The paper is structured as follows. Section 2 describes the model simulations analysed and the particle tracking method. In Section 3 the performance of both models in the Nordic Seas is compared to observations. This is followed by the main results of this study, where the pathways of the NIIC watermass are described in detail in Section 4 and the watermass transformation along the pathways is discussed in Section 5. A discussion and the conclusions are provided in Section 6.

2. Methods

In this study, a Lagrangian analysis is conducted to trace the NIIC watermass. Numerical particles are advected offline using the velocity fields of the model output. The particles' location, depth, temperature and salinity are saved and used to determine the pathways and watermass transformation of the NIIC water. This method is applied to two ocean models that differ substantially in their representation of deep convection and sea ice in order to investigate the sensitivity of the results to the location of deep mixed layers and heat fluxes.

2.1. Global ocean model configurations

The particles are advected in the Modular Ocean Model global ocean-sea ice model (MOM) and the Parallel Ocean Program ocean-only model (POP). The ocean model configurations are described in detail by Spence et al. (2017) (MOM) and Weijer et al. (2012) (POP) and form the ocean component of frequently-used climate models (MOM in GFDL-CM2.6 and POP in CESM1.0). The models have the same horizontal resolution of 0.1° and use a tripolar B-grid. This yields ~ 4.5 km resolution at 65°N . Nurser and Bacon (2014) estimated the first Rossby Radius of deformation to be ~ 7 km in the Norwegian Sea and ~ 3 km in the Iceland and Greenland Sea. Therefore, these ocean models are only partly eddy resolving in the region of interest. In the vertical, MOM (POP) has 50 (42) layers with a resolution of 5 m at the surface up to 200 m (250 m) in the deeper layers.

Both models are forced by prescribed atmospheric conditions using the Coordinated Ocean-ice Reference Experiments Normal Year Forcing (COREv2-NYF) reanalysis data (Griffies et al., 2009; Large and Yeager, 2009). COREv2-NYF provides a climatological mean atmospheric state estimate at 6-h intervals at roughly 2° horizontal resolution. The atmospheric state is converted to ocean surface fluxes by bulk formulae, so there are no air-sea feedbacks. The Normal Year Forcing is derived from 43 years of the interannual varying atmospheric state from 1958 to 2000. Since the same seasonal forcing is applied every year, the interannual variability is small. Using normal year forcing is advantageous for this study as the results will not depend on the release year of the numerical particles. For practical reasons, only one year of velocity data representative for the mean ocean state of the models is used in this study.

The KPP parameterization is used for the parameterization of convection in both models (Large et al., 1994). Further, vertical viscosities and diffusivities are set by KPP and in the horizontal, biharmonic viscosity and diffusion are used. In MOM, the surface salinity is restored on a 60-day timescale. In POP, the surface salinity is restored during the first 75 years of the spin-up period. From that moment onwards, 'mixed boundary conditions' are applied, derived from the monthly-averaged restoring flux of the final five years of the spin-up.

The models differ in their sea-ice configurations. MOM is coupled to the GFDL Sea Ice Simulator model, so the sea ice evolves freely. In POP, the sea-ice edge is fixed and defined by the -1.8°C isotherm of the SST climatology from COREv2-NYF. Under the diagnosed sea ice, temperature and salinity are restored with a timescale of 30 days. The approaches regarding the sea-ice configurations in MOM and POP lead to large differences in the maximum sea-ice extent in the Nordic Seas, as shown by the black line in Figs. 2b and c. In POP the maximum sea-ice extent is confined to the continental shelves of Greenland, whereas in MOM the sea ice covers most of the Greenland and Iceland Seas in winter months. Additionally, Fig. 2 shows that the modeled hydrographic fields of the two models differ as well. Section 3 will further elaborate on these differences with respect to observations.

2.2. Tracking the Atlantic Water north through Denmark Strait

Lagrangian particles are released daily for a duration of one year in the northward flowing Atlantic Water in Denmark Strait. The particles are released at a zonal transect at 66°N between Iceland and 28.9°W (black line in Fig. 1 in Denmark Strait) at a resolution of 0.1° longitude and 20 m in the vertical. The particle is only traced when the initial meridional velocity is positive (hence flowing to the north) and when the initial temperature is higher than 5°C (hence Atlantic Water). Each particle is tagged with its corresponding volume transport that is defined as the meridional velocity multiplied by the area of the cell face in which the particle is released (Döös, 1995).

The particles are advected forward in time with a timestep of 1 h within the daily averages of the 3D velocity field output of the ocean model using the Connectivity Modeling System (CMS) (Paris et al.,

2013). The CMS model uses a tricubic interpolation spatially, and a 4th order Runge Kutta stepping scheme in time. No horizontal or vertical diffusivity is added to the particles, so the particle motion is purely advective. Mixing is only taken into account as far as it is represented by resolved eddies. The CMS model does include the option to parameterize the vertical movement in mixed layers by adding a random kick in the vertical to the particle trajectories (van Sebille et al., 2013). Results of including this option are compared to results without the parameterization, and no significant changes were found in the particle pathways and the watermass transformation along the paths. The change in density of the particles in the convection region defines the future path, as the particles have to follow isopycnals. It does not matter at which depth the particle is located within the mixed layer, since the T-S properties of the mixed layer are continuously homogenized by the convective adjustment used in the model simulations. Therefore, the results of the CMS model without the parameterization of the vertical movement in mixed layers have been used in this study.

In total 226407 (284412) particles are tracked in MOM (POP). The total advection time of the particles is chosen to be 6 years and is executed by looping through the available dataset of one year of model output. The resulting pathways and timeseries of temperature and salinity of the particles do not show large variations from the end of December to the beginning of January, which justifies this method. After six years, the majority of the particles has left the Nordic Seas (81% in MOM and 69.8% in POP, see Section 4 and Fig. 6).

The resulting pathways are then visualized using a particle density plot (see Section 4 and Fig. 5). To this end every particle location is regridded on a $0.1^\circ \times 0.1^\circ$ latitude-longitude grid. Each position can only be occupied by the same particle once, to avoid the obscuration of the pathways by long residence times as described by Behrens et al. (2017). The particle density is given by the transport carried by the particles at each location divided by the total transport. This way, the paths that the particles are most likely to take are highlighted.

3. Model performance in the Nordic Seas

Apart from the different sea-ice configuration and the SSS restoring, the set-up of the two models is very similar, as described in Section 2.1. Still, the resulting hydrography and circulation is remarkably different. In this section, a comparison of the two models is made and the modeled fields are validated against observations to highlight possible consequences of the different model configurations. Also, the interpretation of the findings from the Lagrangian approach in Sections 4 and 5 requires knowledge of the Eulerian background velocity and hydrography. The first part of this section compares the Nordic Seas hydrography and the mixed layer depth from each model to observations. The second part addresses the circulation in both models and the third part discusses the hydrography at the Kögur section (see Fig. 1) to investigate the properties of the NIIC and the Denmark Strait Overflow Water.

3.1. Hydrographic properties

The mean temperature and salinity at 50 m depth of both models is compared to the observed fields of the Nordic Seas from 1995 to 2010 in Fig. 2a-f. A depth of 50 m is chosen, since at this depth the difference in temperature between the eastern and western basins is more pronounced than at the surface. Apart from some local discrepancies, both models compare well to the observed hydrography in the Nordic Seas. The hydrographic fields in MOM differ from the observations on the western side of the Nordic Seas. The Greenland Sea and Iceland Sea are colder than observed ($\Delta T \sim 2^\circ\text{C}$, Fig. 2b) and the waters near the Greenland coast are too fresh ($\Delta S \sim 0.5$ psu, Fig. 2e). In POP, a warm and saline signal that is not present in observations, seems to propagate onto the northern Greenland shelf region at 80°N (Figs. 2c and f). Furthermore, the lateral spread of the Atlantic Water throughout the

Table 1

Mean transport (Ψ), temperature (T) and salinity (S) of the NIIC, DSOW, NIJ and EGC from observations and the model simulations. Observational values are estimated from [1] Våge et al. (2013), [2] Jónsson and Valdimarsson (2005), [3] Pickart et al. (2017), [4] Jochumsen et al. (2017), [5] Eldevik et al. (2009), [6] Harden et al. (2016) and [7] Håvik et al. (2017).

	NIIC			DSOW			NIJ			EGC (76°N)		
	obs	MOM	POP	obs	MOM	POP	obs	MOM	POP	obs	MOM	POP
Ψ (Sv)	1. 1 ^[1]	1.1	1.8	3. 2 ^[4]	2.5	3.1	$1 \pm 0.17^{[6]}$	0.5	1.3	5 – 7 ^[7]	7.5	2.8
T (° C)	3 – 6 ^[2]	6.2	6.6	0.1 – 0. 5 ^[5]	2.5	– 0.5	– 0.4 – 0 ^[3]	1.4	– 0.4	2 – 4 ^[7]	2.3	0.7
S (psu)	35 – 35. 15 ^[3]	35	35.1	34.82 – 34. 94 ^[5]	34.9	35	34.9 – 34. 91 ^[3]	34.9	35	34.9 – 35. 1 ^[7]	34.9	35

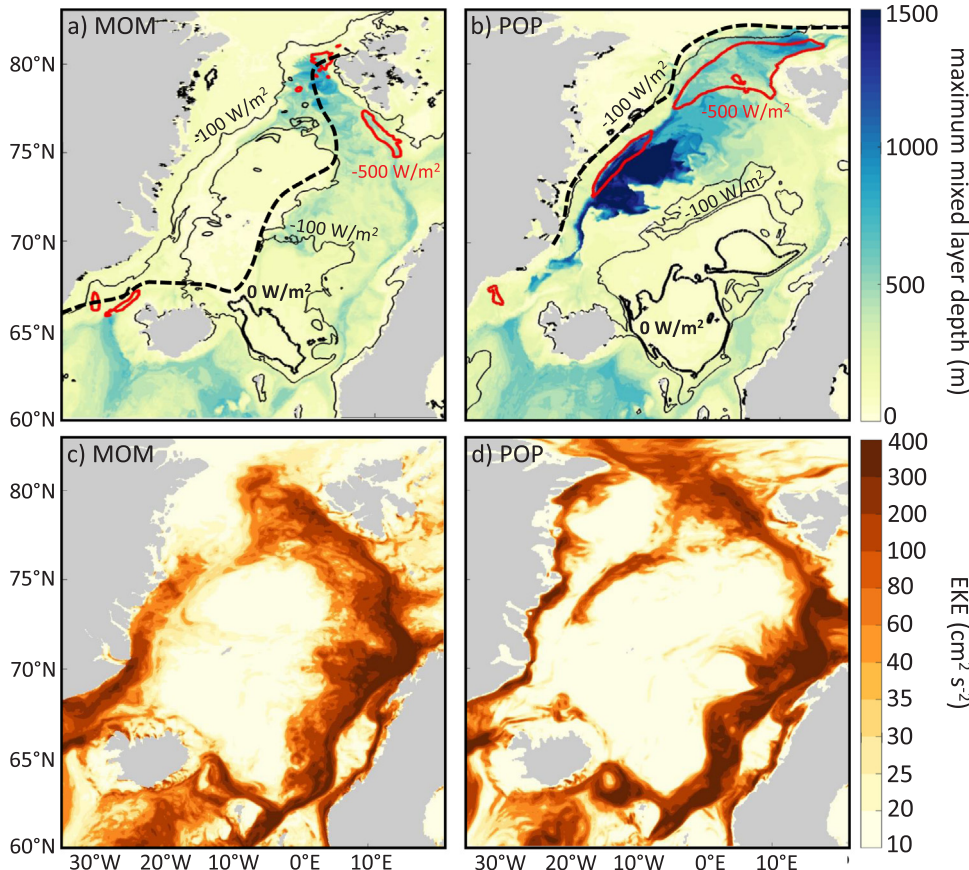


Fig. 3. Maximum mixed layer depth (top) and eddy kinetic energy (bottom) for MOM (left) and POP (right). Solid contours in (a) and (b) show the -500 W/m^2 (in red), -100 W/m^2 and 0 W/m^2 (in black) March mean heat flux. The dashed contours indicate the sea-ice extent in March (For interpretation of the references to color in this figure legend, the reader is referred to the web version of this article).

eastern basins is minimal in POP. Instead, a local minimum in temperature is seen in both the Lofoten Basin and the Norwegian Basin (Fig. 2c). Further, the Atlantic Water returning in the EGC is warmer in MOM than in POP, indicating that the boundary current in POP loses more heat than the boundary current in MOM (see also Table 1).

The location where deep convection takes place in both models is very different. Fig. 3a and 3b show the maximum mixed layer depth (MLD) in MOM and POP. In order to use a common criterion for both models, the MLD is defined as the depth where the density difference compared to the surface is larger than 0.125 kg/m^3 as described in Danabasoglu et al. (2014). The density is determined from the temperature and salinity fields using the UNESCO nonlinear equation of state (Millero and Poisson, 1981). The maximum in MLD is reached at the end of winter and beginning of spring. The models display a clear difference in both the magnitude and the location of deep convection. In MOM the convection reaches 1000 m depth, and the deepest mixed layers are seen southwest of Svalbard and within the Norwegian Atlantic Current (Fig. 3a). In contrast to MOM, POP has mixed layers with a maximum of 1500 m depth along the shelf break of Greenland, into the Greenland Basin and north of the Icelandic Plateau (Fig. 3b).

The location and depth of deep convection are strongly dependent on the atmospheric forcing, the sea ice and the stratification of the water column (e.g. Moore et al., 2015; Harden et al., 2015; Våge et al., 2018). Comparing the location and the depth of the deep convection to the atmospheric heat flux (contours in Fig. 3) and the sea-ice edge in March (dashed lines in Fig. 3) confirms this. In MOM the edge of the deep convection region coincides with the -100 W/m^2 heat flux contour (Fig. 3a). Furthermore, it is clear that the deep convection in the western basin is absent because the sea ice is preventing the cooling of the ocean surface by the atmosphere. In POP the sea-ice edge, which is located much closer to the Greenland coast (see dashed line in Fig. 3b), also plays an important role for the location of the deep convection. The strongest heat fluxes are found along the sea-ice edge, which makes the water column more prone to deep convection.

Observational estimates of the mixed layer depth in the Nordic Seas are limited due to the lack of year-round observational data. Mixed layers with depths of 560 m have been observed in the Lofoten and Norwegian Basins (Nilsen and Falck, 2006; Richards and Straneo, 2015). The deep convection in the Greenland Sea is highly variable and can extend to depths of 2000 m (Rudels et al., 1989; Latarius and

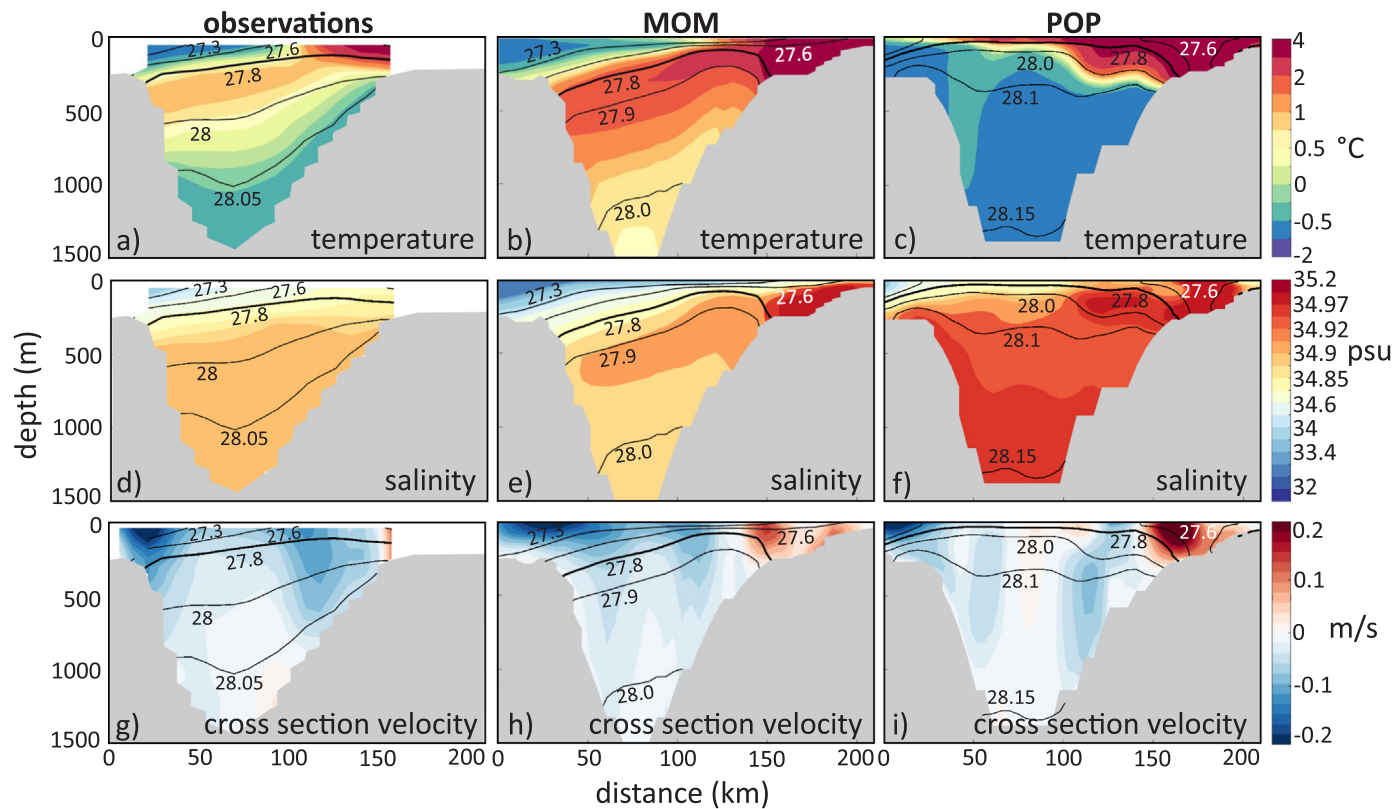


Fig. 4. Sections of temperature (top), salinity (middle) and cross section velocity (bottom) at the Kögur section (transect given in Fig. 1). The x-axis shows the distance along the transect, starting at the Greenland coast. Positive velocity indicates northward flow. The left column shows the mean fields from observations described by Harden et al. (2016). The middle and right column show the mean fields of MOM and POP respectively. Density is given by the contourlines, where the thick black line corresponds to $\sigma = 27.8 \text{ kg/m}^3$. Note that the colorbars for temperature and salinity are non-linear.

(Quadfasel, 2016). Combining all available observational data in the Iceland Sea, Våge et al. (2015) found that the deepest mixed layers in this basin ($\sim 300 \text{ m}$) are located in the northwest, close to Greenland. These findings suggest that the deep convection in the Greenland Sea is better represented in POP and the deep convection in the Lofoten Basin is better represented in MOM. Further, POP overestimates the maximum MLD in the Iceland Sea, whereas in MOM deep convection does not occur in this region. These differences are likely a direct consequence of the difference in sea-ice behavior between the models. Recall that the sea-ice extent in POP is fixed to observed values, whereas in MOM the sea ice is dynamically active. Apparently, the sea-ice model used in MOM is overestimating the sea-ice extent in the Nordic Seas, which suppresses deep convection in the western basins.

3.2. Nordic Seas Circulation

The circulation pattern in the Nordic Seas is strongly controlled by topography, while the strength of the circulation is influenced by the wind forcing and hydrography (e.g. Blindheim and Østerhus, 2005; Spall, 2010). Figs. 2g-i show the mean sea surface height (SSH) from observations, and in MOM and POP. The SSH in both models compares quite well to observations, except in the Lofoten Basin. Especially in POP a depression in SSH is clearly seen in the Lofoten Basin, whereas a positive SSH anomaly is commonly observed in this area associated with the Lofoten Vortex (e.g. Søiland et al., 2016; Fer et al., 2018). The arrows in Figs. 2h and i show the mean surface velocity in both models. The location and direction of the currents compare well to the observed surface circulation derived from drifters by e.g. Jakobsen et al. (2003). The model results differ regarding the strength of the currents. POP has a very strong cyclonic gyre in the Lofoten Basin and the Norwegian Basin, but the circulation in the Greenland and Iceland Basin is weaker.

In MOM cyclonic gyres are most pronounced in the Greenland Basin and the Norwegian Basin. As the EGC in POP is very weak (see also Table 1), most Arctic Water is transported southwards by the East Greenland Coastal Current. In MOM this current is less pronounced.

When the circulation is compared to the structure of deep convection in the basin (Figs. 2h-i to 3a-b), the regions with convective activity coincide with regions of low velocity in both models. This seems contradictory at first, since deep convection in the interior of ocean basins is thought to be positively correlated with the strength of the cyclonic boundary current that is surrounding the basin: as the interior of the ocean basin is cooled during winter, the temperature gradient between the boundary current and the interior increases and the boundary current strengthens as a result of the thermal wind balance (e.g. Spall, 2004; Tréguier et al., 2005). However, in our simulations a strong cooling coincides with a weak temperature gradient between the interior and the boundary current and therefore with a reduced geostrophic transport. The reduced temperature gradient is probably caused by the stronger cooling over the boundary current area compared to the interior. This heat loss seems to be so strong that the supply of warm water from the boundary current upstream is not sufficient and thereby, the boundary current temperature decreases.

The eddy kinetic energy (EKE) is shown in Figs. 3c-d. Although the model resolution is not sufficient to fully resolve all eddy activity in the Nordic Seas, most of the variability is captured. The largest eddy variability is seen west of the Lofoten islands. Here, the EKE exceeds $400 \text{ cm}^2 \text{ s}^{-2}$, which compares relatively well to observational estimates (e.g. Wekerle et al., 2017). North of Iceland a small band of increased EKE from the NIIC can be seen. Both observational estimates of the eddy variability in this region and estimates from higher resolution model simulations show slightly larger values for EKE of $\sim 100 \text{ cm}^2 \text{ s}^{-2}$ compared to $\sim 60 \text{ cm}^2 \text{ s}^{-2}$ in MOM and POP (e.g. Jakobsen et al., 2003;

Wekerle et al., 2017).

3.3. Hydrographic properties at Kögur section

Next, the properties of the inflowing Atlantic Water and the outflowing Overflow Water through Denmark Strait are compared between the models and mooring observations at the Kögur section (Harden et al., 2016). This transect is well documented from observations and the characteristics of both the inflowing NIIC and the outflowing dense waters can be distinguished along the section. Further, to enable direct comparison between the models and observations, Table 1 shows the mean temperature, salinity and volume transport estimates of the NIIC, DSOW, NIJ and EGC.

Fig. 4 shows the mean temperature, salinity and the cross-section velocity (positive indicates northward flow) at the Kögur section. The mean temperature along the Kögur transect in MOM captures the observed pattern well (Fig. 4b), although the deep waters are too warm ($\Delta T \sim 1^\circ\text{C}$, Fig. 4b). In POP, the stratification is much stronger than observed, with warmer water at the surface ($\Delta T \sim +2^\circ\text{C}$) and colder waters below ($\Delta T \sim -1.5^\circ\text{C}$, Fig. 4c). The salinity shows similar discrepancies, where the surface and deep layers are too fresh in MOM and too salty in POP by ~ 0.1 psu compared to the observations (Figs. 4e and f). Combining the findings for temperature and salinity, the in- and outflowing waters in MOM are slightly too light and the in- and outflowing waters in POP are too dense.

In the cross-section velocity at the Kögur section different branches can be distinguished (Figs. 4g-i). The NIIC is present in both models and is characterized by a warm and salty water mass flowing north on the Icelandic shelf. The NIIC transport is 1.1 Sv in MOM and 1.8 Sv in POP compared to 0.88–1.1 Sv estimated from observations (Jónsson and Valdimarsson, 2012; Våge et al., 2013). As a result of the model bias in density, the overflow water is characterized by different isopycnals. The 27.8 kg/m^3 respectively 28.0 kg/m^3 isopycnals are chosen to represent the overflow water mass in MOM and POP. This results in an overflow transport into the Atlantic of 2.4 Sv in MOM and 3.1 Sv in POP, which is slightly lower than the observed estimate of 3.2 Sv from Jochumsen et al. (2017). Compared to observations, the NIJ is better represented in POP than in MOM (see Table 1).

In summary, this section discussed the differences between the models and observations. Overall, the models capture the main characteristics of the Nordic Seas well, but disagree on the location of deep mixed layers, the gyre strength in the Nordic Seas and the hydrographic characteristics of the Denmark Strait Overflow Water. The remainder of this paper will focus on whether these differences influence the pathways of the NIIC water and the location and strength of the watermass transformation.

4. Pathways of the NIIC watermass in the Nordic Seas

The density plot of the particles seeded in the NIIC (see Section 2.2) reveals the pathways of the NIIC watermass in the Nordic Seas (Fig. 5). After entering the Nordic Seas, most particles follow the 400 m isobath around Iceland to the east (see inlays Fig. 5). From there, multiple pathways can be identified following the shelfbreak and the main topographic features of the Nordic Seas; the Vøring Plateau and the Jan Mayen- and Mohn Ridges (see Fig. 1).

These particle density plots show that the paths along which the particles enter the interior of the Nordic Seas are completely different between the two models. Particles mainly occupy the Lofoten Basin in MOM, whereas in POP the particles occupy the Greenland Basin. In MOM, particles are captured by eddies near the Lofoten Islands and travel westward until they reach the Mohn Ridge. There, the majority of the particles flows to the north and eventually joins the EGC. In POP, the particles are not captured by eddies near the Lofoten islands, but are transported in the strong cyclonic gyre of the Lofoten Basin and the Norwegian Basin instead. At the western side of the Nordic Seas,

particles travel throughout the Greenland Basin, without displaying one distinctive path.

The residence time of the particles within the Nordic Seas is highly variable and depends on where the particles leave the basin. The median travel time is given in Fig. 5 for the particles that enter and leave the Nordic Seas within the time interval of 6 years (Section 2.2). The shortest residence times of ~ 1 year are found for particles taking a short path crossing the Greenland-Scotland Ridge, whereas the particles that follow the path along the rim of the Nordic Seas take ~ 4 years to do so. On average, the travel time towards Fram Strait is one year shorter in POP than in MOM, which indicates that the particles flow much faster from the Lofoten Islands to Fram Strait in POP than in MOM.

In order to distinguish between the different paths, particles are selected based on which exit they take out of the Nordic Seas. This particle categorization process is illustrated in Fig. 6a. Furthermore, a selection is made based on whether particles enter the interior of the Nordic Seas, or stay close to the boundary with respect to the coastlines of Iceland, Norway, Svalbard and Greenland. Although the categorization is sensitive to the choice of the transects shown in Fig. 6a, inspection of the individual particle trajectories indicates that the transect locations used in this study lead to a meaningful separation.

The result of this categorization process is summarized by Figs. 6b and c. In both models, most of the NIIC watermass leaves the Nordic Seas toward the Atlantic Ocean by crossing the Greenland-Scotland Ridge (66.7% in MOM and 42.5% in POP). A smaller fraction of the NIIC watermass flows into the Arctic via Fram Strait or the Barents Sea (14.3% in MOM and 27.3% in POP). The part of the NIIC water that takes longer than 6 years to leave the Nordic Seas (19% in MOM and 30.2% in POP) is found mostly in the interior of the basin (not shown). A much longer advection time would be needed to advect all of the originally seeded NIIC particles out of the Nordic Seas.

The particles leaving the Nordic Seas through Denmark Strait can do so following different paths as indicated in Figs. 6b-c; via a short loop north of Iceland (the DSs, short, path), via the rim of the Nordic Seas (the DSL, long, path), via the interior of the Nordic Seas (the DSM, middle, path) and via the coastal shelf area of Greenland (the DSc, coastal, path). As the connection of the NIIC to the overflow is the main interest of this study, the remainder of this paper is focused on the NIIC water returning to the Atlantic Ocean. Although the sea-ice cover, the mixed layers, and the transport of the NIIC show a seasonal dependence in the two model simulations, the pathways of the NIIC watermass are not sensitive to the time of release of the particles.

Both models show the existence of a short loop along the inflowing NIIC back to Denmark Strait (the DSs path). At first sight, this path seems similar to the hypothesized path of Våge et al. (2011). However, only 13% of the volume that entered the Nordic Seas in the NIIC is taking this path in both MOM and POP, in contrast to the fast one-to-one connection between the NIIC and the NIJ proposed by Pickart et al. (2017). Furthermore, investigation of the particles' depth is needed in order to see whether this outward branch is actually part of the NIJ. To this end, the vertical distribution of the in- and outflowing branches of the different pathways at the Kögur section are visualized in Figs. 7a and b. To derive this figure, the particles crossing this transect are mapped on a $0.1^\circ \times 10 \text{ m}$ longitude-depth grid. Only the contour that encompasses more than 80 % of the particles is shown to highlight the main position of each pathway in the watercolumn.

In both models, most of the DSs watermass originates from the upper 100 m of the NIIC (solid pink contour in Figs. 7a-b), and this path is therefore shallower than the other paths. The particles follow the shelf break of Iceland and turn northwards at Kolbeinsey Ridge. In MOM, the particles return to Denmark Strait following the 1000 m isobath along the Icelandic slope. In POP, some particles circulate in the Bloseville Basin (Fig. 1) as well. On their outward journey, there is no indication in MOM that the DSs particles are connected to the NIJ, since the returning particles are all located in the upper 100 m of the water

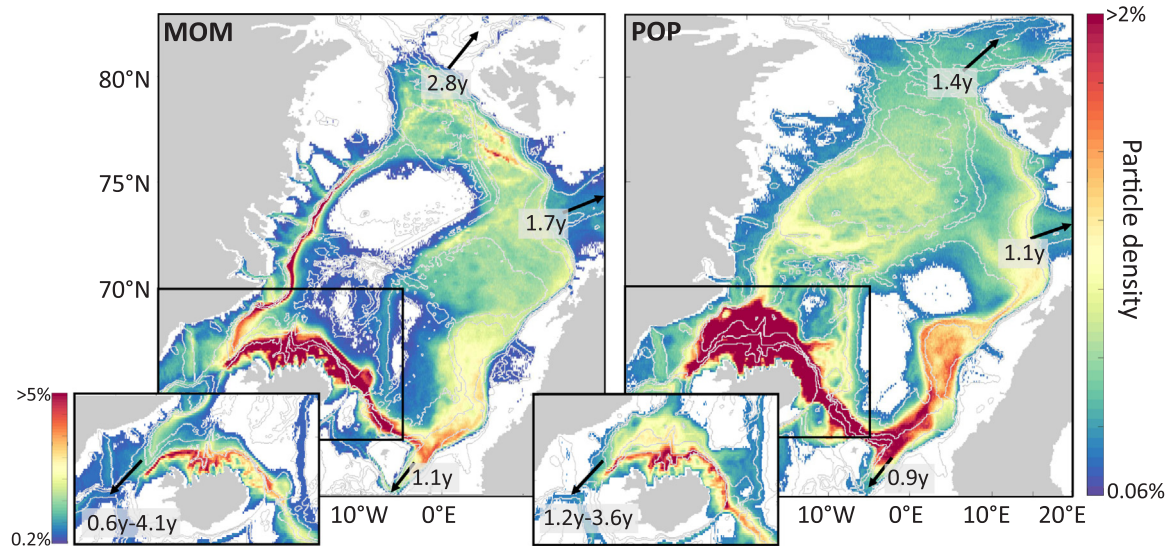


Fig. 5. Density plot of the particle position in MOM (left panel) and POP (right panel). The inlay shows the pathways near Iceland in more detail (note the different colorscale in the bottom left). The median travel time for the particles to reach the exits of the Nordic Seas is given in years.

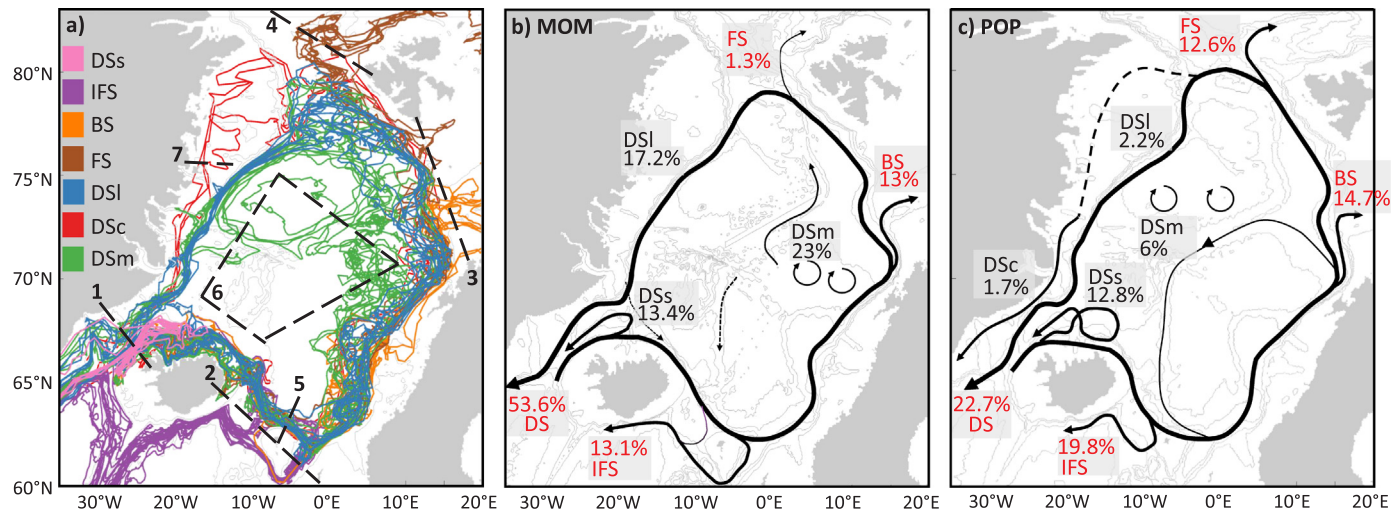


Fig. 6. (a) Example of 63 randomly chosen particle trajectories from both MOM and POP and their categorization (color coding). DSs (Denmark Strait short, pink) are particles that leave the Nordic Seas crossing transect 1, without crossing transect 5. IFS particles (Iceland-Faroe-Shetland, purple) are particles that leave by crossing transect 2. BS (Barents Sea, orange) are particles that travel into the Barents Sea crossing transect 3. FS (Fram Strait, brown) are particles that travel into the Arctic Ocean by crossing transect 4. DSI (Denmark Strait long, blue) are particles that travel along the rim of the Nordic Seas, crossing transects 5 and 1. DSc (Denmark Strait coast, red) are particles that follow the same route as DSI, but travel on the shelf region of Greenland crossing transect 7. DSM (Denmark Strait middle, green) are particles that enter the interior of the Nordic Seas indicated by box 6 and leave the Nordic Seas through transect 1. (b-c) The black arrows indicate the paths of the NIIC water in the Nordic Seas where the percentage gives the distribution of the NIIC watermass over the different pathways. The total fraction of the NIIC watermass that leaves through each exit is given in red. 19% (30.2%) of the particles are still in the Nordic Seas after 6 years in MOM (POP) (For interpretation of the references to color in this figure legend, the reader is referred to the web version of this article).

column (pink dashed line in Fig. 7a). In POP, however, there is a clear signal of outward flowing particles between 200 m and 400 m depth close to the Icelandic slope (pink dashed line Fig. 7b), showing that in this model the outward branch is part of the NIJ. This indicates that the watermass transformation of the particles following the DSs path is different in both models. This will be further discussed in Section 5.

As only 13% of the NIIC watermass takes the DSs path, the majority of the water is transported by other paths. A significant fraction of the NIIC watermass leaves the Nordic Seas between Iceland and the Shetland islands in both models (the IFS path, 13% in MOM and 20% in POP). In POP, all of the IFS particles leave the Nordic Seas between Iceland and the Faroe Islands (the IF path), whereas in MOM the majority of the IFS particles (> 60%) leaves through the deeper channel between the Faroe Islands and Scotland (the FaS path). Again, the

vertical distribution of the pathways is investigated by mapping the particles on a $0.1^\circ \times 10\text{ m}$ latitude-depth grid of a transect east of Iceland (Fig. 7c and d). Clearly, the IFS particles (purple color in Fig. 7c-d) are located deeper in the water column than the particles of the other pathways. In MOM, the particles leaving between the Faroe Islands and Scotland are located slightly farther offshore. Therefore, they follow the 1000 m isobath to the Faroe-Shetland Channel. The possible connection of the IFS path to the Iceland Scotland Overflow Water (ISOW) will be discussed in Section 5.

Investigation of the vertical distribution of the pathways at the Kögur section and the transect east of Iceland gives insight why some particles flow south (the IFS path) and why some flow northward east of Iceland (the BS, FS, DSM, DSI and DSc paths). At the start of their trajectory, the maximum concentration of the particles that do not take

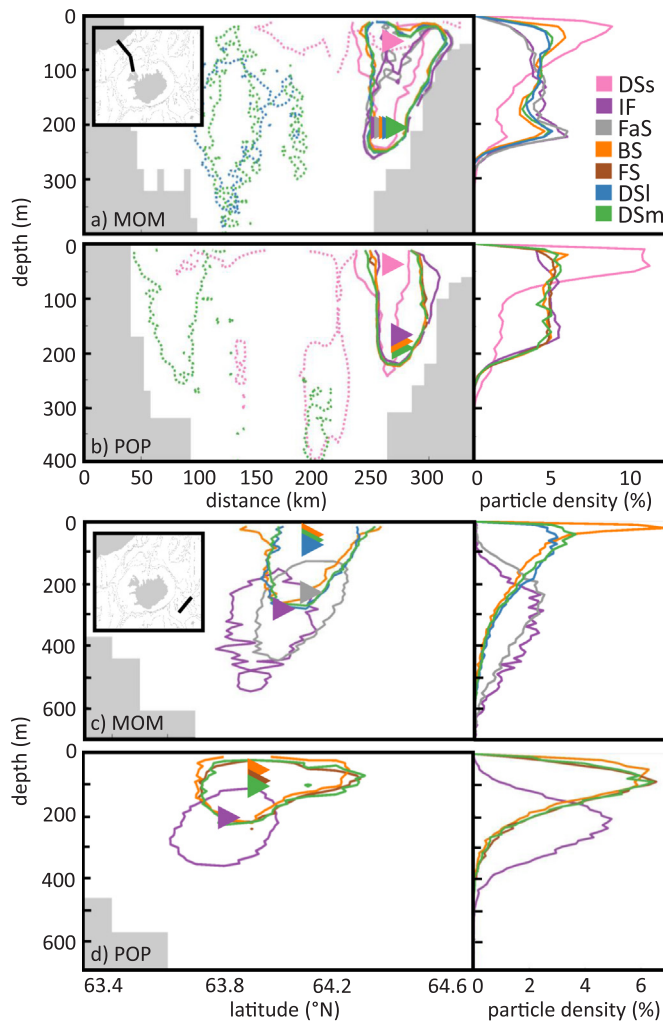


Fig. 7. The depth distribution of each pathway at (a,b) Kögur section and (c,d) a section east of Iceland (see inlays). The left panels show the contour, colored per pathway, that encompasses > 80% of the particles. The triangles give the location where the maximum particle concentration of the pathway is found at these transects. The solid contours show the distribution of the particles that flow into the Nordic Seas, the dashed lines show the distribution of the pathways on their outward journey. The right panels show the normalized depth distribution of each path integrated along the transects. The IFS particles are separated in those that leave the Nordic Seas between Iceland and the Faroe Islands (IF, in purple) and those that leave the Nordic Seas between the Faroe Islands and Scotland (FaS, in gray). Only the paths that carry more than 5% of the NIIC water are shown (For interpretation of the references to color in this figure legend, the reader is referred to the web version of this article).

the DSs path is found at 200 m depth in both models (see triangles in Figs. 7a and b). However, east of Iceland, the particles that continue their journey north are all shifted upwards in the water column, whereas most particles that flow south are found below 200 m depth (compare the purple and gray contours to the other colors in Fig. 7c and d). The upper part of the water column east of Iceland is characterized by the Atlantic Water flowing north in the NwAC. Particles that are located near the surface are therefore likely to mix with the inflowing Atlantic Water and flow north, whereas the deeper particles follow the topography to the south.

These results indicate that processes that take place between the two investigated transects are crucial for setting the ratio of the southward and northward flowing fraction of the NIIC. The instability of the NIIC in this region (see Fig. 3c-d) could provide one possible mechanism for setting these pathways apart. The generation of eddies

coincides with local up- and downward movement of isopycnals and this process could separate particles in depth (Ypma et al., 2016). Another possible mechanism is that the particles are set apart in depth by local mixing within the mixed layer, which influences their density. It is beyond the scope of this study to determine the dominant processes in this region that are important for the transformation of the NIIC watermass. However, it is likely that the ratio of the southward and northward flowing fraction of the NIIC is subject to interannual variability.

The particles that flow north in the NwAC can take different routes. They either flow into the Barents Sea, flow through Fram Strait or return south along Greenland to Denmark Strait. One of the main differences between MOM and POP is that more than half of the NIIC watermass leaves through Denmark Strait in MOM, where most particles take the long way around (along the DSL and DSM paths). In POP, only 23% leaves through Denmark Strait, which may be explained by the weak EGC in POP and the long residence time of the particles in the Greenland Basin. Using a longer advection time of the particles would possibly increase the fraction of the NIIC watermass leaving the Nordic Seas through Denmark Strait in POP.

In summary, according to the two model simulations investigated in this study the connection between the NIIC and the NIJ is either weak (in POP) or non-existent (in MOM). Furthermore, the model simulations suggest a possible connection between the NIIC and the ISOW.

5. Watermass transformation along the pathways

In order to investigate the watermass transformation along the pathways of the NIIC water in the Nordic Seas, the temperature and salinity are traced for each particle. As an example, Fig. 8a shows the trajectory of one of the particles that takes the DSL route in POP. Along this path, a net cooling and freshening of 7°C and 0.13 psu is seen (Fig. 8b), leading to an increase in density of 0.68 kg/m^3 . The transformation predominantly takes place at times when the particle is located inside the mixed layer (shaded periods in Figs. 8b and c). Note that the magnitude of the cooling that takes place is not necessarily related to the depth of the mixed layer, neither to the strength of the heat flux at the surface. As seen in Fig. 8b between location 1 and 2, the particle changes its thermohaline properties to a warmer and saltier watermass, while traveling to a location with a deeper mixed layer and a stronger atmospheric cooling. Most likely, the warming and increase in salinity is a result of mixing with Atlantic Waters that enter the Nordic Seas east of Iceland. Two periods of strong cooling along the path of the particle can be distinguished. The cooling that takes place north of Iceland (upstream of number 1 in Fig. 8a) at the start of the trajectory coincides with a reduction in salinity. This could indicate another mixing process with cold and fresh waters from the north. The second cooling event takes place when the particle is south of Svalbard (between location 6 and 7 in Fig. 8a). During this cooling event, the salinity change is rather small and the particle is close to the sea surface, indicating that the reduction in temperature is most likely due to atmospheric cooling.

Note that, not only this particle, but all particles change their density predominantly, when they are located within the mixed layer. This is because diapycnal mixing below the mixed layer is small (e.g. Ledwell et al., 1993). In the model simulations, diapycnal mixing originates from the vertical background diffusion and in case of steep fronts from horizontal biharmonic diffusion. In addition to diapycnal mixing, there can be isopycnal mixing (mixing of temperature and salinity without a change in density) either by the explicitly resolved eddies or by horizontal diffusion. However, the effect of isopycnal mixing on temperature and salinity is much smaller than the diapycnal and diabatic water mass transformation within the ocean mixed layers. This is evident in Fig. 8b-c from the much smaller temperature and salinity changes when the particle is below the mixed layer.

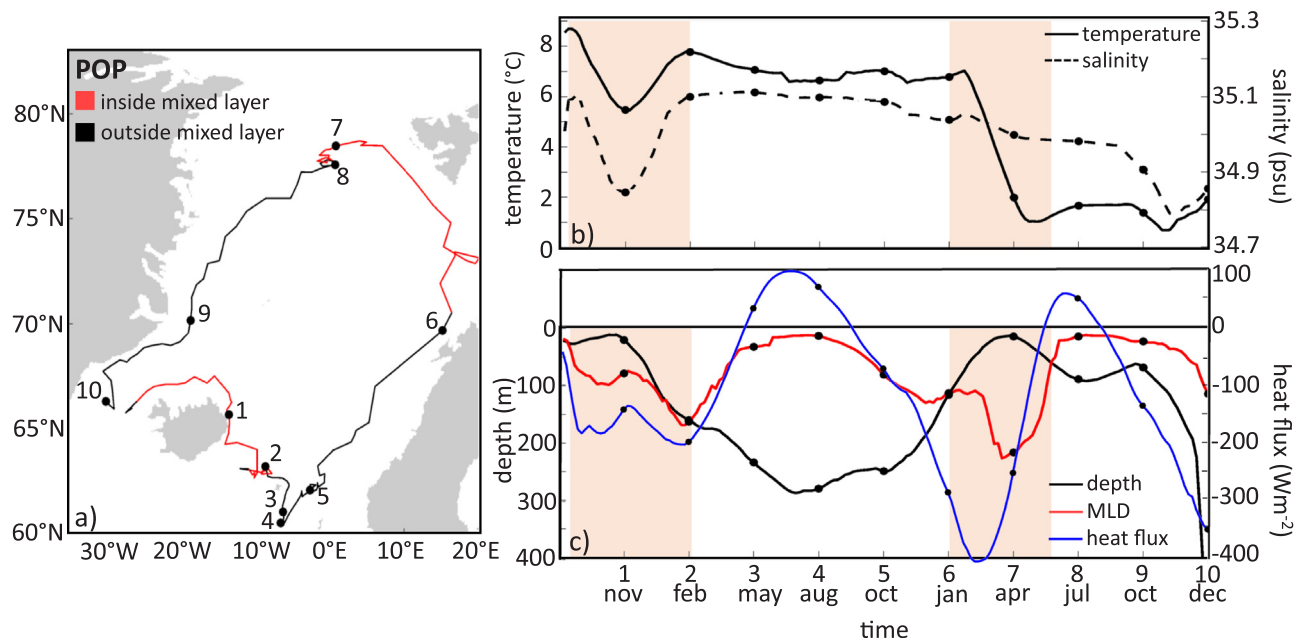


Fig. 8. (a) Example trajectory of a DSL particle in POP that is part of the DSOW. The line is red where the particle is traveling inside the mixed layer, the line is black outside the mixed layer. (b) Temperature (solid black line, left axis) and salinity (dashed black line, right axis) along the path of the particle trajectory shown in panel a. (c) Depth of the particle (in black), the mixed layer depth along the trajectory (in red) and the heat flux at the sea surface along the trajectory (in blue, negative means cooling). The shaded orange periods in (b-c) indicate when the particle is in the mixed layer. The numbers along the time axis of panel b and c correspond to the numbers in panel a, showing the particle location at the specified time (For interpretation of the references to color in this figure legend, the reader is referred to the web version of this article).

5.1. Contribution of the NIIC water to overflow waters

The investigation of this single particle pathway already elucidates many aspects of density changes that can occur in the Nordic Seas. To analyze the watermass transformation of the NIIC and its contribution to the overflows, all particles need to be taken into account. The change in temperature and salinity of the particles is visualized in the T-S diagrams in Figs. 9a and b, where T-S properties of the particles that enter the Nordic Seas (in green) are compared to the T-S properties of the particles that exit the Nordic Seas at either Denmark Strait, crossing the Iceland-Scotland Ridge, into the Barents Sea or through Fram Strait (in purple). The temperature and salinity of the particles is gridded on a $\Delta T = 0.1^\circ \text{C}$ and $\Delta S = 0.05 \text{ psu}$ temperature-salinity grid. In both models a clear shift to lower temperatures is seen ($\Delta T \sim 4\text{--}7^\circ \text{C}$) and little change in salinity.

Using the thermohaline properties of the particles, an estimate can be made to what extent the NIIC watermass contributes to the overflow waters in both models. Figs. 9c and d show the mean volume transport of all the water crossing Denmark Strait as a function of temperature and salinity for MOM and POP, derived from the Eulerian mean velocity fields. The thick density contour shows the minimum density of the overflows defined in Section 3.3. The same contour is also shown in Figs. 9a and b. Using this threshold density, 27% (14.7%) of the water transported by the NIIC reaches a density that is larger than 27.8 kg/m^3 (28.0 kg/m^3) when leaving the Nordic Seas in MOM (POP).

To investigate along which paths this dense water is transported, the outflow temperature and salinity of the particles is split over five T-S categories, indicated by the gray lines in Figs. 9a-b. The categories are based on whether the density along the pathway increased sufficiently to resemble the overflow (category 1), whether both temperature and salinity decreased (category 2), whether mainly the salinity decreased (category 3), whether the temperature increased (category 4), or whether the thermohaline properties of the particles remained roughly similar (category 5).

Applying this categorization process to each pathway (Fig. 10) directly reveals along which pathways the dense water that eventually

contributes to the overflows is transported (blue color in Fig. 10). In MOM, the NIIC water that contributes to DSOW is transported mainly via the DSL and DSm path (18.2%, 0.20 Sv). In POP, 10.8% (0.19 Sv) of the NIIC water reaches Denmark Strait as DSOW, which is mainly transported via the DSS pathway and partly by the DSm path.

The NIIC watermass is also connected to the overflow between Iceland and Scotland (ISOW) in both models via the IFS path, and this connection is stronger in MOM than in POP (7.8%, 0.09 Sv in MOM and 2.1%, 0.04 Sv in POP). In MOM, the majority of the IFS particles are transformed to the overflow density (blue color Fig. 10), whereas in POP most particles have T-S properties that are similar to those at entering the Nordic Seas (gray color Fig. 10). However, just before entering the Iceland-Faroe Channel (at the transect shown in Figs. 7c-d), the T-S properties of the particles in POP are very similar to those in MOM (not shown). A possible explanation for the sudden decrease in density is the slightly deeper mixed layer depths in the Iceland-Faroe Channel found in POP, making the IFS watermass more prone to mixing with the warm and salty Atlantic Water layer. This is linked to the fact that the IFS particles in MOM leave mainly through the deep channel east of the Faroe Islands, whereas the IFS particles in POP leave west of the Faroe Islands (Section 4). In both models the isopycnal that serves as the upper threshold for the overflow waters is located at $\sim 500 \text{ m}$ depth at the Iceland-Scotland Ridge. As the channel between Iceland and the Faroe Islands is only 500 m deep, most of the ISOW has to leave east of the Faroe Islands, where the channel is 1100 m deep.

Most of the particles that flow into the Barents Sea show either similar temperatures or an increase in temperature with respect to their original properties when flowing into the Nordic Seas. As a result, both simulations show only few particles with an overflow density entering the Barents Sea and the Arctic Ocean (1% in MOM and 1.8% in POP). It is likely that a part of the watermass that enters the Barents Sea and the Arctic Ocean will transform to denser waters further north, but this is outside the scope of this study.

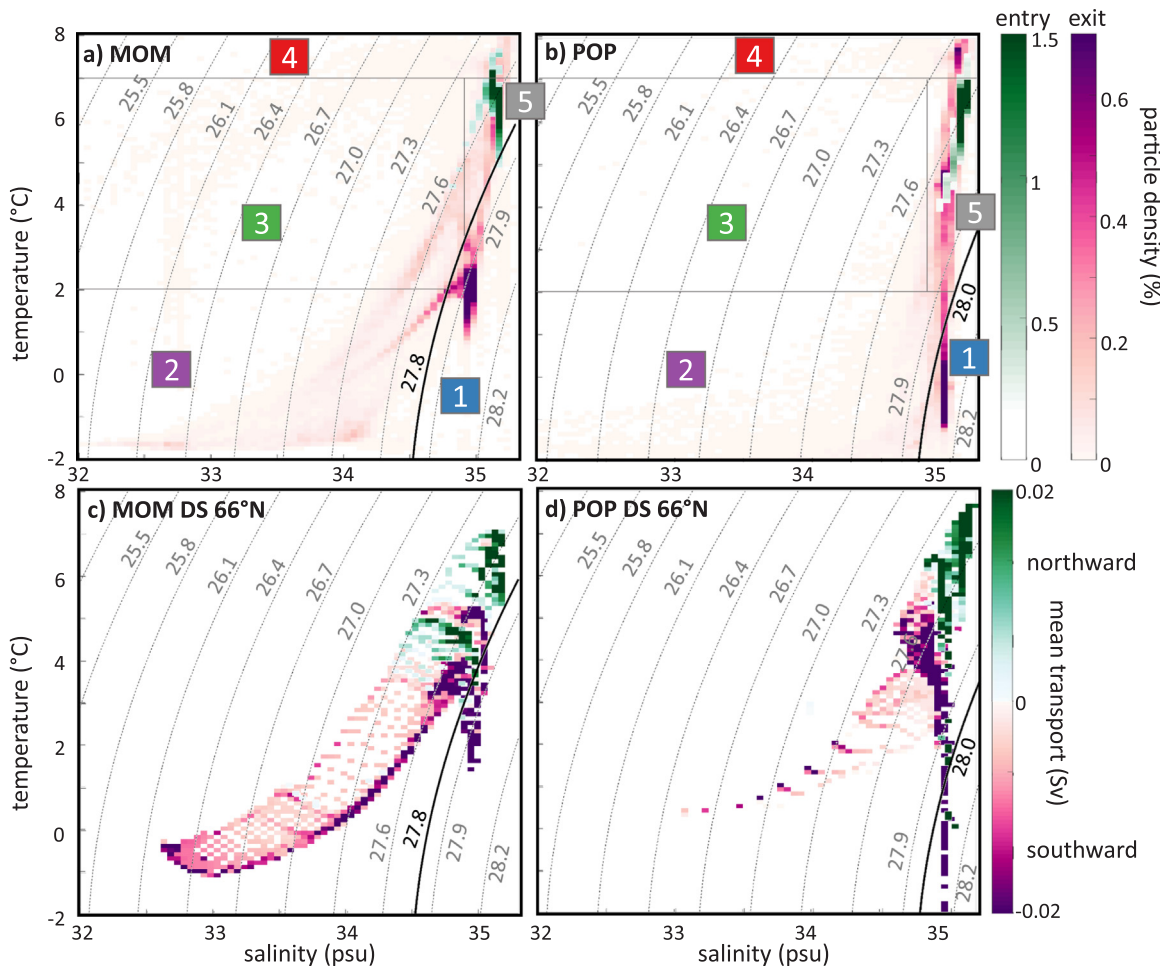


Fig. 9. (a-b) T-S diagrams of the thermohaline properties of the particles when entering the Nordic Seas (in green) and exiting the Nordic Seas at any of the exit locations (in purple) for (a) MOM and (b) POP. The transport weighted particle density is shown per $\Delta T = 0.1^\circ \text{C}$ and $\Delta S = 0.05 \text{ psu}$ interval. The horizontal and vertical gray lines separate the T-S categories used in Fig. 10. (c-d) Mean volume transport from the Eulerian velocity fields at Denmark Strait (66° N) as a function of temperature and salinity in MOM (left) and POP (right). Transport into the Nordic Seas is shown in green and transport out of the Nordic Seas in purple. In all panels, contours are density (kg/m^3), where the thick black line indicates the density threshold for the overflow waters (see Section 3.3) in MOM respectively POP (For interpretation of the references to color in this figure legend, the reader is referred to the web version of this article).

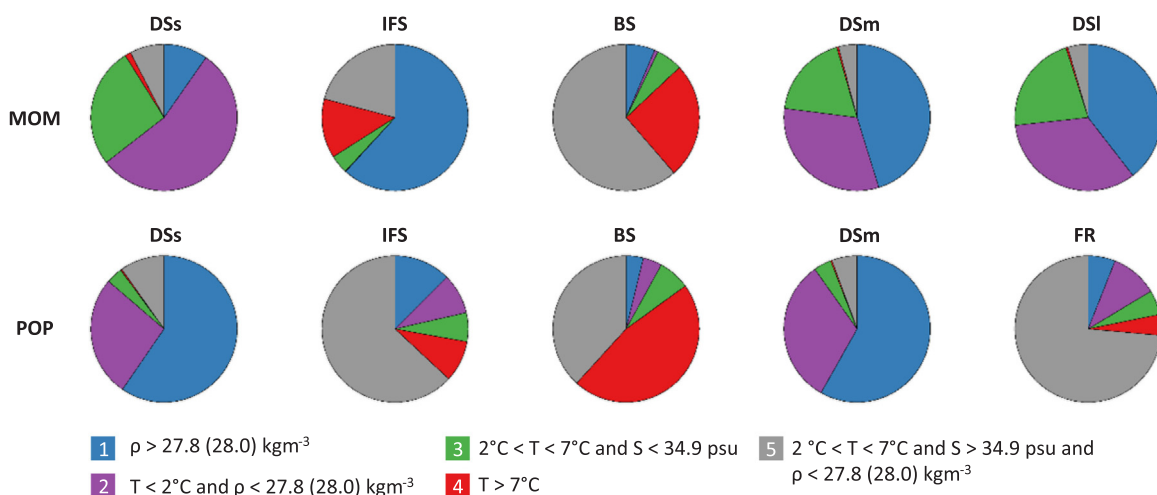


Fig. 10. Fraction of particles per pathway leaving the Nordic Seas within specific T-S categories, described in Figs. 9a-b. Only the paths that carry more than 5% of the NIIC water are shown.

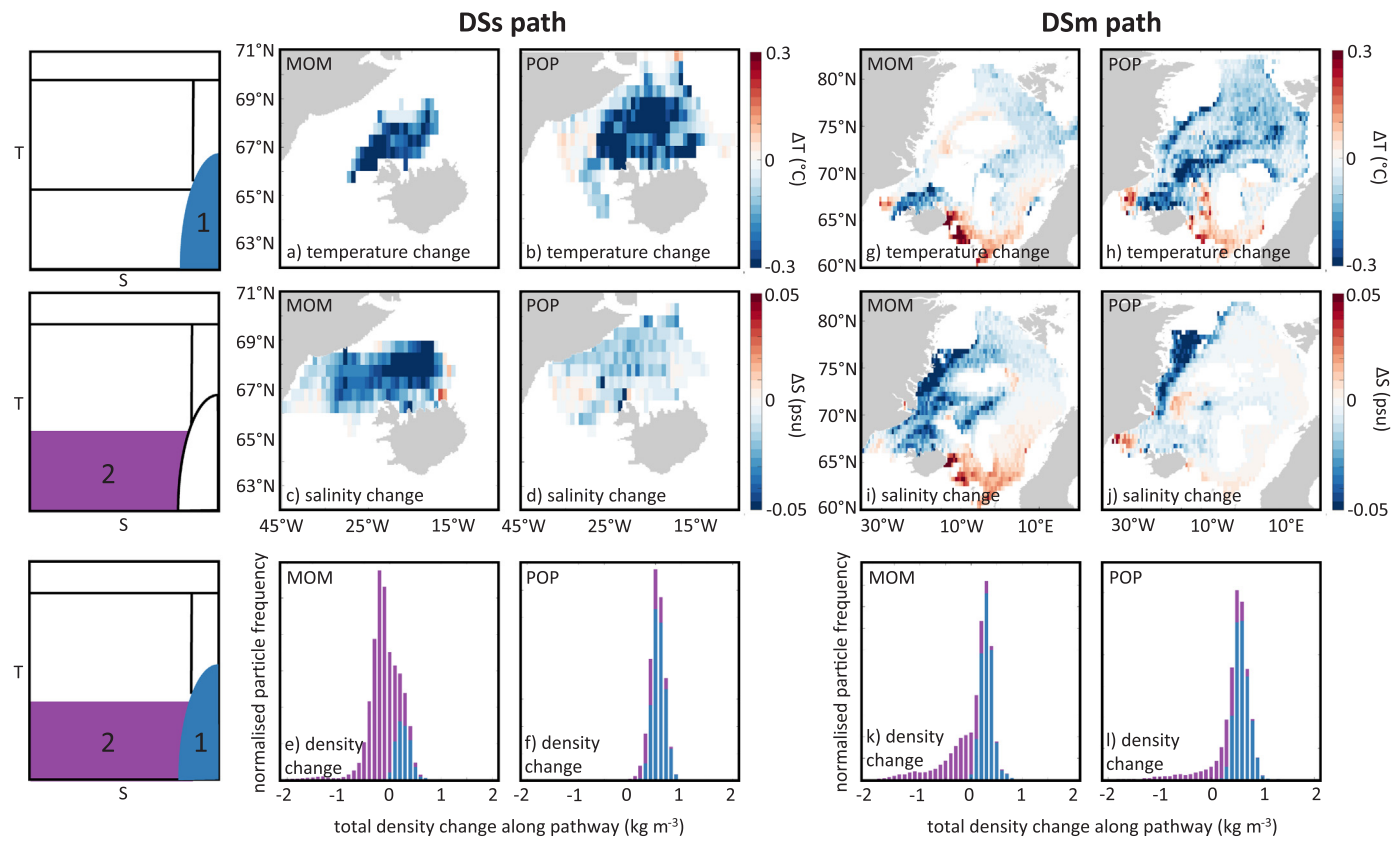


Fig. 11. Temperature change per $0.5 \times 0.5^\circ$ lon-lat gridbox (a-b, g-h), salinity change per $0.5 \times 0.5^\circ$ lon-lat gridbox (c-d, i-j) and total density change (e-f, k-l) along the DSs path (a-f) and the DSm path (g-l). The upper row shows the temperature change of the particles whose density at leaving the Nordic Seas is larger than 27.8 (28.0) kg/m^3 (T-S category 1, see Figs. 9 and 10). The middle row shows the salinity change of the particles whose temperature and density properties at leaving the Nordic Seas are smaller than respectively 2°C and 27.8 (28.0) kg/m^3 (T-S category 2, see Figs. 9 and 10). The third row shows the distribution of the total density change of each particle along the pathway (positive indicates a density increase), with the particles that connect to the DSOW (T-S category 1) in blue and the particles that leave the Nordic Seas with the T-S properties of T-S category 2 in purple (For interpretation of the references to color in this figure legend, the reader is referred to the web version of this article).

5.2. Location of watermass transformations

To shed more light on the differences and similarities between the two model simulations regarding the watermass transformation along the paths, the location of the thermohaline changes along the pathways is investigated (Fig. 11). The rate of change of temperature and salinity is determined and spatially binned on a $0.5^\circ \times 0.5^\circ$ latitude-longitude grid. Next, this rate of change is multiplied by the residence time of the particles at each gridbox, to obtain the total change in temperature and salinity that the particles undergo at each location. Then, the results are averaged at every gridbox when the particle number in the gridbox exceeds 100 particles.

The watermass transformation along the DSs path displays the largest difference between the two simulations. In MOM, the majority of the particles change their thermohaline properties to a fresher watermass (purple area Fig. 10), whereas in POP a strong transformation to a cold and salty watermass takes place (blue area Fig. 10). Figs. 11a-b show the temperature change for the particles that leave the Nordic Seas as DSOW. Both simulations show strong cooling. In MOM, this cooling is confined to the region just north of Iceland, whereas in POP the water flowing along the DSs path cools over the entire area between Iceland and Greenland.

The differences between both model results become more apparent in Figs. 11c-d, where the salinity change is shown for the particles that change their thermohaline properties to a colder and fresher watermass (T-S category 2, purple area Fig. 10). Where in MOM the strongest cooling is found directly at the release location of the particles (66°N , Fig. 11a), the strongest freshening takes place further downstream (~

68°N , Fig. 11c). In POP, the reduction in salinity is significantly smaller and takes place closer to the Greenland coast (Fig. 11d). The total density change along the DSs pathway (Figs. 11e-f) indicates that the decrease in salinity in MOM outweighs the temperature decrease and most of the DSs particles become lighter along this path. In POP, the salinity decrease is small and most of the particles become denser along the DSs path (Fig. 11f). This explains why the DSs particles are found at the surface in MOM and at depth in POP, when flowing south through Denmark Strait (Figs. 7a-b).

The changes seen in the particles' properties along the DSs path can be related to the location of the sea ice (Figs. 3a-b). As the maximum sea-ice edge extends to the center of Denmark Strait in MOM, cooling by the atmosphere is confined to the region close to Iceland as seen in Fig. 11a. In POP, the region between Iceland and Greenland is ice free year-round, and atmospheric cooling is not hindered by sea ice. Further, it is likely that mixing takes place with the cold and fresh waters that flow south along the Greenland coast. In MOM, the salinity gradient in the Denmark Strait region is much larger than in POP (see Figs. 2e-f). The fresher surface waters seen in MOM can be due to the ice melt, but also due to the different surface freshwater boundary conditions. Therefore, similar mixing will lead to a stronger freshening in MOM than in POP.

The pathway along which the total density change is similar in both simulations is the DSm path (Figs. 10 and Figs. 11k-l). However, the locations where the thermohaline changes take place are different. In MOM, the strongest cooling is found just north of Iceland, similar to the DSs path (Fig. 11g), while in POP, cooling is also seen along the shelfbreak of Greenland and in the interior of the Nordic Seas

(Fig. 11h). Both models show freshening along the Greenland coast, where the water mixes with the Polar Water of the EGC (Figs. 11i-j). In MOM, freshening is also seen just southeast of the Greenland Basin.

Both MOM and POP display local maxima of watermass transformation in the interior of the Nordic Seas (cooling in POP and freshening in MOM, Figs. 11h-i). As seen in Figs. 2h-i the flow speed is significantly lower in the interior of the Nordic Seas than at the boundaries and therefore the local maxima seen in Figs. 11h-i are a result of the larger residence time of the particles in these areas. Just like for the DSs path, the atmospheric cooling is limited by the sea-ice extent over the western side of the Nordic Seas in MOM as seen in Fig. 11g and the freshening southwest of the Greenland Basin is likely a result of ice melt. The model simulations show an increase in both temperature and salinity southeast of Iceland. This transformation is a result of mixing with the Atlantic Water that flows into the Nordic Seas east of Iceland (Fig. 1). The location of watermass transformation along the other pathways was investigated as well, but did not differ substantially from the watermass transformation along the DSm path shown in Fig. 11g-j.

In summary, both simulations show a similar contribution of the NIIC to the DSOW of 0.2 Sv. However, the pathways along which the transformation takes place differ. This is a result of the differences in sea-ice cover in the Nordic Seas, and likely due to the different freshwater boundary conditions of the model simulations. As hypothesized in Section 4, investigation of the thermohaline properties of the particles elucidated a weak connection between the NIIC and the ISOW.

6. Discussion and conclusions

In this paper Lagrangian particles have been used to investigate the pathways and the watermass transformation of the North Icelandic Irminger Current (NIIC) in the Nordic Seas in two ocean models. The volume of the NIIC water along each pathway and the contribution of the NIIC watermass to Denmark Strait Overflow Water (DSOW) and Iceland Scotland Overflow Water (ISOW) have been quantified. Further, the locations of the watermass transformation have been studied to investigate their relation to the location of the convection regions within the Nordic Seas.

Based on observations, some studies propose a strong connection between the NIIC and the DSOW, where the NIIC watermass is transformed northwest of the Iceland gyre and flows back into the Atlantic Ocean via the North Icelandic Jet (NIJ) through Denmark Strait (Våge et al., 2011; Pickart et al., 2017). The indication that both currents carry a similar volume transport and the assumption that the EIC does not contain a large part of the NIIC watermass, led to a suggested one-to-one connection between the NIIC and the NIJ (e.g. Pickart et al., 2017). The results from this study provide a different view than that deduced from the observations. The models suggest that the inflowing NIIC watermass is divided over several pathways in the Nordic Seas, and that only 13% of the NIIC watermass flows till Kolbeinsey Ridge to follow the short suggested loop. The region north of Iceland seems to play a crucial role in diversifying these pathways. The connection from the NIIC to DSOW via the NIJ has only been found in POP, since in MOM strong freshening takes place near the surface.

As was shown in Fig. 7, the particles that follow the short DSs path originate from the upper 100 m of the NIIC, whereas the deeper part of the NIIC flows farther east along Iceland. This could explain why Valdimarsson and Malmberg (1999) concluded that the DSs path was the main route for the NIIC, since this was the only path they could observe using surface drifters. Jónsson (1992) observed the NIIC watermass at the northeast corner of Iceland, slightly deeper in the watercolumn. In light of the results of our study, it is possible that he measured the fraction of the NIIC watermass that eventually leaves between Iceland and Scotland (the IFS path). Both models used in this study show a very strong watermass transformation north of Iceland. Therefore it is possible that observations underestimate the Atlantic Water originating from the NIIC east of Iceland. Also, the part of the

NIIC water that travels offshore of Iceland is indistinguishable from the EIC. Therefore, this study fits well with previous work that concluded that the EGC is most likely not the only source for the EIC (e.g. Logemann et al., 2013).

The results of this study strongly indicate that the DSs path is topographically controlled and that the fraction of the NIIC water following this path is set by the vertical structure of the current. Our results indicate that the path itself is not sensitive to sea-ice cover and atmospheric conditions and hence it is likely that similar conclusions can be drawn when repeating this research in models with inter-annually varying forcing. Further, as the instability of the NIIC is only slightly underestimated in the model simulations presented in this study, it is not expected that a fully eddy-resolving simulation would show a significantly stronger connection between the NIIC and the NIJ.

Both models display only 0.2 Sv NIIC contribution to the Denmark Strait Overflow Water, although the paths along which this water is transported back to Denmark Strait differ. This means that in these models the NIIC can not be the main source for the NIJ watermass. This is in line with the Lagrangian analysis conducted previously by Behrens et al. (2017), who found that only a small part of the DSOW originated from the NIIC. Note that as their study concerned only backtracking of the DSOW, no statement could be made on what fraction of the NIIC watermass contributes to the overflow as is done in this study.

Interestingly, both MOM and POP show a small contribution of the NIIC watermass to the ISOW of 7.8% respectively 2.1%, which is a weak connection that might be hard to detect by observations (e.g. Stefánsson, 1962; Perkins et al., 1998). Part of the Modified East Icelandic Water originates from the North Icelandic Shelf and is formed during winter convection and modified due to strong mixing with surrounding watermasses (Stefánsson, 1962; Read and Pollard, 1992). It is likely that the IFS path found in the models resembles this contribution.

The model simulations used in this study show agreement on both the pathways of the NIIC watermass and the contribution to the overflows, regardless of the large differences in the sea-ice cover, the hydrography and the circulation patterns between the simulations. This gives confidence that the conclusions drawn from the simulations regarding the NIIC pathways are not a model artifact, but apply to actual processes in the Nordic Seas.

The models do show some differences regarding the pathways along which DSOW is created. The agreement between the models in the NIIC contribution to DSOW of 0.2 Sv could therefore be a pure coincidence. In MOM, a mean freshening is seen along the DSs path and dense water is only transported to Denmark Strait along the deeper part of the EGC by the DSl and DSm paths. In POP, the EGC is weak and is only reached by a limited number of particles (2.2%). However, since the DSs path in POP does not display a strong decrease in salinity, this pathway serves as the main connection between the NIIC and the DSOW in this model.

The models have a very different approach regarding the sea ice, which might explain why the watermass transformation to DSOW is different. The sea-ice cover in MOM between Greenland and Iceland is substantial and in POP non-existent (see black lines Figs. 2b and c). Therefore, the strong freshening seen in MOM along the DSs path could be a result of sea-ice melt northwest of Iceland. Also the strength of the EGC seems to be affected by the location of the sea ice. It could be that a reduction in the sea ice in MOM would lead to a smaller decrease in salinity along the DSs path, leading to a larger contribution to DSOW. At the same time, the reduction in sea ice might lead to a stronger cooling of the EGC by the atmosphere which could resolve into a reduction of this current as is seen in POP. These relations are hypothetical and require further research outside the scope of this paper. What this study does show is that while the DSOW transport might be well captured by ocean models, the path of the dense water to Denmark Strait is highly sensitive to the hydrographic properties of the modeled ocean circulation.

In conclusion, this paper has shown that the connection between the

North Icelandic Irminger Current and the Denmark Strait Overflow Water in MOM and POP is not as strong as proposed by observations. Furthermore, this paper confirms that the NIIC is connected to the Iceland Scotland Overflow Water as well. The watermass transformations taking place north of Iceland and the vertical structure of the NIIC play a crucial role in setting the future pathways of the NIIC watermass. The pathways along which the dense water is formed is different between the two models, highlighting the sensitivity to the model's representation of the hydrography and circulation in the Nordic Seas.

Acknowledgments

S.L. Ypma, S. Georgiou and N. Brüggemann were supported by NWO (Netherlands Organisation for Scientific Research) VIDI grant 864.13.011 awarded to C.A. Katsman. P. Spence was supported by an ARC DECRA Fellowship DE150100223. H.A. Dijkstra acknowledges support by the Netherlands Earth System Science Centre (NESSC), financially supported by the Ministry of Education, Culture and Science (OCW), Grant no. 024.002.001. Computing services for the MOM simulations were provided by the National Computational Infrastructure (NCI) in Canberra, Australia. Use of the SURFsara computing facilities for the POP simulations was sponsored by the Netherlands Organization for Scientific Research (NWO-E) under the project 15502. The model data used in the analyses in this paper has been described in [Spence et al. \(2017\)](#) (MOM) and [Weijer et al. \(2012\)](#) (POP). The observational dataset at the Kögur section was made available by Benjamin Harden. The altimeter products were produced by Ssalto/Duacs and distributed by Aviso+, with support from Cnes (<https://www.aviso.altimetry.fr>). We would like to thank five anonymous reviewers whose helpful comments greatly improved this paper.

References

- Behrens, E., Våge, K., Harden, B., Biastoch, A., Böning, C.W., 2017. Composition and variability of the Denmark Strait Overflow Water in a high-resolution numerical model hindcast simulation. *J. Geophys. Res.: Oceans* 122, 2830–2846.
- Blindheim, J., Østerhus, S., 2005. The Nordic Seas, main oceanographic features. In: *The Nordic Seas: An Integrated Perspective*, pp. 11–37.
- Courtois, P., Hu, X., Pennelly, C., Spence, P., Myers, P.G., 2017. Mixed layer depth calculation in deep convection regions in ocean numerical models. *Ocean Model.* 120, 60–78.
- Danabasoglu, G., Yeager, S.G., Bailey, D., Behrens, E., Bentsen, M., Bi, D., Biastoch, A., Böning, C., Bozec, A., Canuto, V.M., et al., 2014. North Atlantic simulations in coordinated ocean-ice reference experiments phase II (CORE-II). Part I: mean states. *Ocean Model.* 73, 76–107.
- Döös, K., 1995. Interocean exchange of water masses. *J. Geophys. Res.: Oceans* 100, 13499–13514.
- Eldevik, T., Nilsen, J.E.Ø., Iovino, D., Olsson, K.A., Sandø, A.B., Drange, H., 2009. Observed sources and variability of Nordic Seas overflow. *Nat. Geosci.* 2, 406.
- Fer, I., Bosse, A., Ferron, B., Bouruet-Aubertot, P., 2018. The dissipation of kinetic energy in the Lofoten Basin Eddy. *J. Phys. Oceanogr.* 48, 1299–1316.
- Fetterer, F., Knowles, K., Meier, W., Savoie, M., Windnagel, A.K., 2017. Sea Ice Index, Version 3, Boulder, Colorado USA. NSIDC: National Snow and Ice Data Center.
- Griffies, S.M., Biastoch, A., Böning, C., Bryan, F., Danabasoglu, G., Chassignet, E.P., England, M.H., Gerdes, R., Haak, H., Hallberg, R.W., et al., 2009. Coordinated ocean-ice reference experiments (COREs). *Ocean Model.* 26, 1–46.
- Hansen, B., Østerhus, S., 2000. North Atlantic-Nordic Seas exchanges. *Prog. Oceanogr.* 45, 109–208.
- Harden, B.E., Renfrew, I.A., Petersen, G.N., 2015. Meteorological buoy observations from the central Iceland Sea. *J. Geophys. Res.: Atmos.* 120, 3199–3208.
- Harden, B.E., Pickart, R.S., Valdimarsson, H., Våge, K., de Steur, L., Richards, C., Bahr, F., Torres, D., Børve, E., Jónsson, S., et al., 2016. Upstream sources of the Denmark Strait Overflow: observations from a high-resolution mooring array. *Deep Sea Res. Part I: Oceanogr. Res. Pap.* 112, 94–112.
- Håvik, L., Pickart, R., Våge, K., Torres, D., Thurnherr, A., Beszczynska-Möller, A., Walczowski, W., von Appen, W.J., 2017. Evolution of the East Greenland Current from Fram Strait to Denmark Strait: synoptic measurements from summer 2012. *J. Geophys. Res.: Oceans*.
- Jakobsen, P.K., Ribergaard, M.H., Quadfasel, D., Schmitt, T., Hughes, C.W., 2003. Near-surface circulation in the northern North Atlantic as inferred from Lagrangian drifters: variability from the mesoscale to interannual. *J. Geophys. Res.: Oceans* 108.
- Jochumsen, K., Moritz, M., Nunes, N., Quadfasel, D., Larsen, K.M., Hansen, B., Valdimarsson, H., Jonsson, S., 2017. Revised transport estimates of the Denmark Strait overflow. *J. Geophys. Res.: Oceans* 122, 3434–3450.
- de Jong, M.F., Søiland, H., Bower, A.S., Furey, H.H., 2018. The subsurface circulation of the Iceland Sea observed with RAFOS floats. *Deep Sea Res. Part I: Oceanogr. Res. Pap.*
- Jónsson, S., Valdimarsson, H., 2005. The flow of Atlantic water to the North Icelandic Shelf and its relation to the drift of cod larvae. *ICES J. Mar. Sci.* 62, 1350–1359.
- Jónsson, S., Valdimarsson, H., 2012. Water mass transport variability to the North Icelandic shelf, 1994–2010. *ICES J. Mar. Sci.* 69, 809–815.
- Jónsson, S., 1992. Sources of fresh water in the Iceland Sea and the mechanisms governing its interannual variability. In: *Proceedings of ICES Marine Science Symposia*, pp. 62–67.
- Köhler, A., 2010. Variable source regions of Denmark Strait and Faroe Bank Channel overflow waters. *Tellus A* 62, 551–568.
- Koralev, A., Baranova, O.K., Smirnov, A.D., Seidov, D., Parsons, A.R., 2014. Climatological atlas of the Nordic Seas and northern North Atlantic.
- Langehaug, H.R., Medhaug, I., Eldevik, T., Otterå, O.H., 2012. Arctic/Atlantic exchanges via the subpolar gyre. *J. Clim.* 25, 2421–2439.
- Large, W.G., Yeager, S., 2009. The global climatology of an interannually varying air-sea flux data set. *Clim. Dyn.* 33, 341–364.
- Large, W.G., McWilliams, J.C., Doney, S.C., 1994. Oceanic vertical mixing: a review and a model with a nonlocal boundary layer parameterization. *Rev. Geophys.* 32, 363–403.
- Latarius, K., Quadfasel, D., 2016. Water mass transformation in the deep basins of the Nordic Seas: analyses of heat and freshwater budgets. *Deep Sea Res. Part I: Oceanogr. Res. Pap.* 114, 23–42.
- Ledwell, J.R., Watson, A.J., Law, C.S., 1993. Evidence for slow mixing across the pycnocline from an open-ocean tracer-release experiment. *Nature* 364, 701.
- Logemann, K., Ólafsson, J., Snorrason, Á., Valdimarsson, H., Marteinsdóttir, G., 2013. The circulation of Icelandic waters - a modelling study. *Ocean Sci. Discuss.* 10.
- Millero, F.J., Poisson, A., 1981. International one-atmosphere equation of state of seawater. *Deep Sea Res. Part A: Oceanogr. Res. Pap.* 28, 625–629.
- Moore, G.W.K., Våge, K., Pickart, R.S., Renfrew, I.A., 2015. Decreasing intensity of open-ocean convection in the Greenland and Iceland seas. *Nat. Clim. Change* 5, 877.
- Nilsen, J.E.Ø., Falck, E., 2006. Variations of mixed layer properties in the Norwegian Sea for the period 1948–1999. *Prog. Oceanogr.* 70, 58–90.
- Nurser, A., Bacon, S., 2014. The Rossby radius in the Arctic Ocean. *Ocean Sci.* 10, 967–975.
- Paris, C.B., Helgers, J., Van Sebille, E., Srinivasan, A., 2013. Connectivity modeling system: a probabilistic modeling tool for the multi-scale tracking of biotic and abiotic variability in the ocean. *Environ. Model. Softw.* 42, 47–54.
- Perkins, H., Hopkins, T., Malmberg, S.A., Poulain, P.M., Warn-Varnas, A., 1998. Oceanographic conditions east of Iceland. *J. Geophys. Res.: Oceans* 103, 21531–21542.
- Pickart, R.S., Spall, M.A., Torres, D.J., Våge, K., Valdimarsson, H., Nobre, C., Moore, G., Jonsson, S., Mastropole, D., 2017. The North Icelandic Jet and its relationship to the North Icelandic Irminger Current. *J. Mar. Res.* 75, 605–639.
- Read, J., Pollard, R., 1992. Water masses in the region of the Iceland-Faeroes Front. *J. Phys. Oceanogr.* 22, 1365–1378.
- Richards, C.G., Straneo, F., 2015. Observations of water mass transformation and eddies in the Lofoten Basin of the Nordic seas. *J. Phys. Oceanogr.* 45, 1735–1756.
- Rudels, B., Quadfasel, D., Friedrich, H., Houssais, M.N., 1989. Greenland Sea convection in the winter of 1987–1988. *J. Geophys. Res.: Oceans* 94, 3223–3227.
- Søiland, H., Chafik, L., Rossby, T., 2016. On the long-term stability of the Lofoten Basin Eddy. *J. Geophys. Res.: Oceans* 121, 4438–4449.
- Spall, M.A., 2004. Boundary currents and watermass transformation in marginal seas. *J. Phys. Oceanogr.* 34, 1197–1213.
- Spall, M.A., 2010. Non-local topographic influences on deep convection: an idealized model for the Nordic Seas. *Ocean Model.* 32, 72–85.
- Spence, P., Holmes, R.M., Hogg, A.M., Griffies, S.M., Stewart, K.D., England, M.H., 2017. Localized rapid warming of West Antarctic subsurface waters by remote winds. *Nat. Clim. Change* 7, 595.
- Stefánsson, U., 1962. North Icelandic waters. *Atvinnudeild Háskóla Íslands, Fiskideild.*
- Straneo, F., 2006. Heat and freshwater transport through the central Labrador Sea. *J. Phys. Oceanogr.* 36, 606–628.
- Swift, J.H., Aagaard, K., 1981. Seasonal transitions and water mass formation in the Iceland and Greenland seas. *Deep Sea Res. Part A: Oceanogr. Res. Pap.* 28, 1107–1129.
- Tréguier, A.M., Theetten, S., Chassignet, E.P., Penduff, T., Smith, R., Talley, L., Beismann, J., Böning, C., 2005. The North Atlantic subpolar gyre in four high-resolution models. *J. Phys. Oceanogr.* 35, 757–774.
- Våge, K., Pickart, R.S., Spall, M.A., Valdimarsson, H., Jónsson, S., Torres, D.J., Østerhus, S., Eldevik, T., 2011. Significant role of the North Icelandic Jet in the formation of Denmark Strait overflow water. *Nat. Geosci.* 4, 723.
- Våge, K., Pickart, R.S., Spall, M.A., Moore, G., Valdimarsson, H., Torres, D.J., Erofeeva, S.Y., Nilsen, J.E.Ø., 2013. Revised circulation scheme north of the Denmark Strait. *Deep Sea Res. Part I: Oceanogr. Res. Pap.* 79, 20–39.
- Våge, K., Moore, G.W.K., Jónsson, S., Valdimarsson, H., 2015. Water mass transformation in the Iceland Sea. *Deep Sea Res. Part I: Oceanogr. Res. Pap.* 101, 98–109.
- Våge, K., Papritz, L., Håvik, L., Spall, M.A., Moore, G., 2018. Ocean convection linked to the recent ice edge retreat along east Greenland. *Nat. Commun.* 9, 1287.
- Valdimarsson, H., Malmberg, S.A., 1999. Near-surface circulation in Icelandic waters derived from satellite tracked drifters. *Rit Fisk.* 16, 23–40.
- van Sebille, E., Spence, P., Mazloff, M.R., England, M.H., Rintoul, S.R., Saenko, O.A., 2013. Abyssal connections of Antarctic Bottom Water in a Southern Ocean state estimate. *Geophys. Res. Lett.* 40, 2177–2182.
- Weijer, W., Maltrud, M., Hecht, M., Dijkstra, H., Kliphus, M., 2012. Response of the Atlantic Ocean circulation to Greenland Ice Sheet melting in a strongly-eddy ocean model. *Geophys. Res. Lett.* 39,
- Wekerle, C., Wang, Q., Danilov, S., Schourup-Kristensen, V., von Appen, W.J., Jung, T., 2017. Atlantic Water in the Nordic Seas: locally eddy-permitting ocean simulation in a global setup. *J. Geophys. Res.: Oceans* 122, 914–940.
- Willebrand, J., Barnier, B., Böning, C., Dieterich, C., Killworth, P.D., Le Provost, C., Jia, Y., Molines, J.M., New, A.L., 2001. Circulation characteristics in three eddy-permitting models of the North Atlantic. *Prog. Oceanogr.* 48, 123–161.
- Ypma, S., van Sebille, E., Kiss, A., Spence, P., 2016. The separation of the East Australian Current: a Lagrangian approach to potential vorticity and upstream control. *J. Geophys. Res.: Oceans* 121, 758–774.